CHEMISTRY OF MATERIALS

Article

pubs.acs.org/cm

Electron-Deficient *N*-Alkyloyl Derivatives of Thieno[3,4-*c*]pyrrole-4,6-dione Yield Efficient Polymer Solar Cells with Open-Circuit Voltages > 1 V

Julien Warnan,[†] Clément Cabanetos,[†] Romain Bude,[†] Abdulrahman El Labban,[†] Liang Li,[‡] and Pierre M. Beaujuge*,[†]

[†]Physical Sciences and Engineering Division, [‡]Imaging and Characterization Core Laboratory, King Abdullah University of Science and Technology (KAUST), Thuwal 23955-6900, Saudi Arabia

Supporting Information

ABSTRACT: Poly(benzo[1,2-b:4,5-b′]dithiophene−thieno-[3,4-*c*]pyrrole-4,6-dione) (PBDTTPD) polymer donors yield some of the highest open-circuit voltages (V_{OC}, ca. 0.9 V) and fill factors (FF, ca. 70%) in conventional bulk-heterojunction (BHJ) solar cells with PCBM acceptors. Recent work has shown that the incorporation of ring substituents into the side chains of the BDT motifs in PBDTTPD can induce subtle variations in material properties, resulting in an increase of the BHJ device V_{OC} to ∼1 V. In this contribution, we report on the synthesis of *N*-alkyloyl-substituted TPD motifs (TPD(CO)) and show that the electron-deficient motifs can further lower both the polymer LUMO and HOMO levels, yielding device V_{OC} > 1 V (up to ca. 1.1 V) in BHJ solar cells with PCBM. Despite the high V_{OC} achieved (i.e., low polymer HOMO), BHJ devices cast from TPD(CO)-based polymer donors can reach power conversion efficiencies (PCEs) of up to 6.7%, making these promising systems for use in the high-band-gap cell of tandem solar cells.

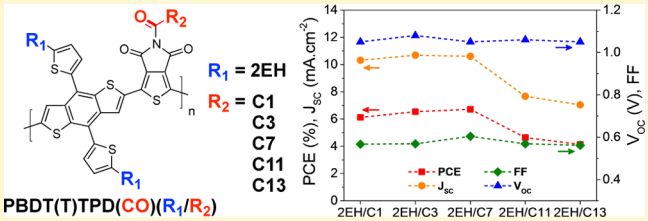

INTRODUCTION

Relying on donor−acceptor principles, polymers of electron-rich benzo[1,2-*b*:4,5-*b*′]dithiophene (BDT) and electron-deficient thieno[3,4-*c*]pyrrole-4,6-dione (TPD) motifs (E_{opt} ∼ 1.9 eV) are some of the most efficient polymer donors in bulk-heterojunction (BHJ) solar cells with fullerene acceptors, such as phenyl-C61/C71-butyric acid methyl ester (PCBM).[1] With power conversion efficiencies (PCEs) > 8% and fill factors (FF) of ca. 70% recently reported in conventional BHJ devices,[2] PBDTTPDs are outstanding candidates for use in the high-band-gap cell of tandem solar cells. In PBDTTPD polymers, the BDT donors set a large ionization potential (IP) of ca. 5.3 eV (i.e., expected low-lying HOMO), which contributes toward high device V_{OC} values > 0.9 V.[3] Importantly, in these systems, varying the size and branching of the solubilizing side chains appended to the π-conjugated main chain impacts polymer self-assembly in thin-film devices, and in turn, BHJ solar cell efficiency.[2,4] Thus, the determining role of side-chain substituents on polymer performance is currently at the forefront of solar cell material optimization studies.[1,5−8]

In recent studies, we and other groups have examined the effect of ring substituents incorporated into the side chains of BDT motifs on polymer properties and BHJ efficiency.[9−13] In PBDT(X)TPD polymers for which the heterocyclic substituents are either furan (X = F), thiophene (X = T), or selenophene (X = S), the choice of the side group can induce subtle changes in material properties and molecular interactions with PCBM acceptors, affecting the thin-film morphologies of the BHJs and yielding distinct PCEs in optimized solar cells.[13] However, it is worth noting that polymer donors involving BDT(X) motifs all yield relatively high device V_{OC} values, independent of the choice of the ring substituent.[9,10,13−16] For example, conventional BHJ solar cells made with PBDT(T)-TPD and PCBM reach a V_{OC} of up to ∼1 V, while the devices maintain high PCEs within the range of 6−6.5%.[13,17] In contrast, several other "high-V_{OC}" polymers have been shown to yield low device photocurrents and poor solar cell efficiencies in BHJs with PCBM, and the ability to develop efficient high-V_{OC} systems has remained a matter of debate for some time.[3,18,19] In fact, recent work has emphasized the detrimental role of inefficient back hole transfer from the fullerene to the polymer donor in BHJ solar cells with V_{OC} values over 1 V—excitons recombining on the fullerene—leading to low internal quantum efficiencies (IQEs), and greatly reduced device photocurrents and FFs.[3]

In this report, we show that PCBM-based BHJ solar cells made from polymers of BDT(T) and *N*-alkyloyl-substituted TPD motifs (TPD(CO)) (Chart 1) can combine high PCEs of up to 6.7% and high V_{OC} > 1 V (up to 1.1 V). Despite their large IPs and the high V_{OC} achieved in BHJs with PCBM, optimized solar cells with PBDT(T)TPD(CO) polymers yield relatively high short-circuit currents (J_{SC}) on the order of 10

Received: January 21, 2014
Revised: April 2, 2014
Published: April 3, 2014

   dx.doi.org/10.1021/cm5002303 | Chem. Mater. 2014, 26, 2829−2835

Chart 1. Molecular Structures of PBDTTPD, PBDT(X)TPD (with X = F, T, or S), and the *N*-Alkyloyl Derivative PBDT(X)TPD(CO)

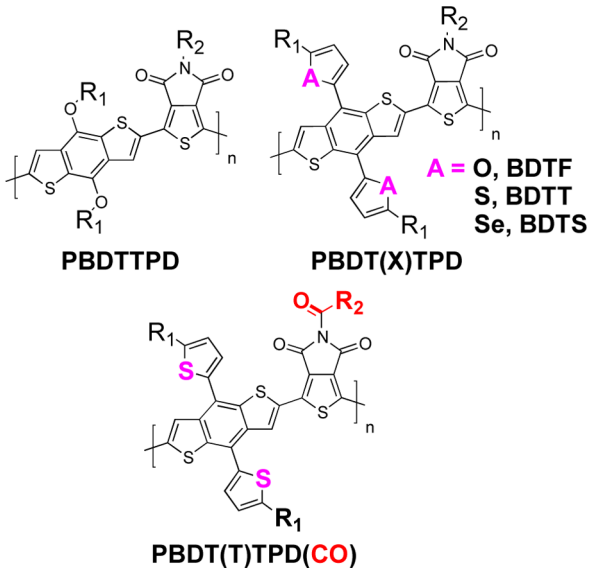

mA cm^{-2} and FFs within the range of 55−60%. We find that solution-processing additives, such as 1-chloronaphthalene (CN) used in the casting solutions, play a key role in setting the adequate BHJ morphology for efficient solar cells with PBDT(T)TPD(CO) polymers.

RESULTS AND DISCUSSION

Design and Synthesis. Electron-deficient thieno[3,4-*c*]pyrrole-4,6-dione (TPD) motifs are promising alternatives to the thieno[3,4-*b*]thiophene (TT) motifs[20−23] in polymer donors for BHJ solar cells with PCBM acceptors. Compared to the 5−7 steps required to prepare electron-deficient TT motifs, the synthesis of TPD units can be achieved in only 3−4 steps.[2,4,24,25] However, TPD motifs have not shown the level of synthetic modularity achievable with TT analogues thus far.[20−23] On the basis of earlier work with TT motifs appended with various upper-ring substituents,[20] the synthesis and incorporation of *N*-alkyloyl-substituted TPD motifs (TPD(CO)) into polymer donors could account for lower-lying LUMO and HOMO levels, affording tunable device V_{OC} values in BHJ solar cells with PCBM.

In recent work,[2] we showed that, for polymers with branched alkyl-substituted BDT motifs, a fine modulation of the number of aliphatic carbons in linear *N*-alkyl-substituted TPD motifs (i) induces significant variations in polymer solubility, and (ii) can be a contributor to improved material performance. To examine this effect in PBDT(T)TPD(CO), TPD(CO) motifs with methyl(C1), propyl(C3), heptyl(C7), undecyl(C11), and tert-decyl(C13) linear chains were prepared sequentially. The *N*-alkyloyl derivatives of TPD (TPD(CO)) (**3**) were synthesized in two steps starting from the 4,6-dibromothieno-[3,4-*c*]furan-1,3-dione (**1**) (Scheme 1a). First, the imide intermediate **2** was prepared by addition of ammonia (NH_3) on the anhydride precursor **1** in anhydrous tetrahydrofuran (THF), and subsequent condensation in the presence of oxalyl chloride (yield: ca. 60%). Next, the imide **2** was treated with sodium hydride (NaH) and subsequently reacted with the desired acyl chloride (R_2COCl). Synthetic details and characterization data are provided in the Supporting

Scheme 1. Syntheses of the BDT(T) and TPD(CO) Motifs

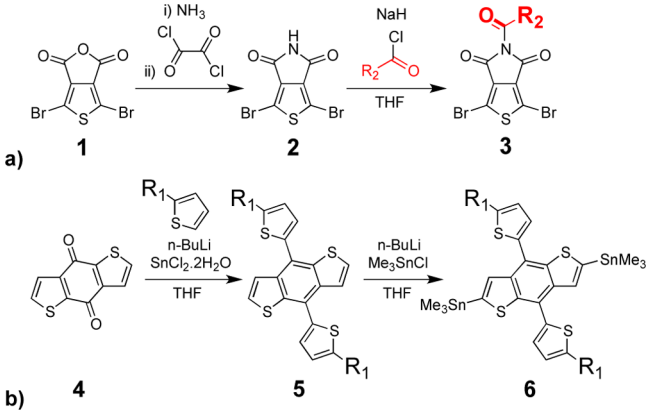

Information. Separate, recent work describes an alternative route to the preparation of TPD(CO).[26] Figure 1 depicts the molecular conformation of a C3-substituted TPD(CO) motif (**3**) resolved by single-crystal X-ray diffraction (see details in the Supporting Information), indicating that a torsion angle of 20.6° exists between the carbonyl of the *N*-alkyloyl group and the molecular plane of TPD (Figure 1c). The thiophene-substituted BDT(T) motif **6** was synthesized by addition of lithiated 2-(2-ethylhexyl)thiophene on the precursor **4** in THF. The trimethyltin moieties were installed by deprotonation with *n*-BuLi at −78 °C and subsequent quenching of the lithiated intermediate with trimethyltin chloride ($SnMe_3Cl$) (Scheme 1b). Similar protocols have been used in recent studies for the synthesis of various BDT(X) units.[9,11,14,16,27−31] Recent work has emphasized the relevance of thiophene-substituted benzo-[1,2-*b*:4,5-*b*′]dithiophene (BDT(T)) as a motif in the preparation of polymer donors that yield high V_{OC} ∼ 1 V in BHJ solar cells with PCBM.[9,13] The PBDT(T)TPD(CO) polymers (Scheme 2) were synthesized by a microwave-assisted approach (150 °C for 1 h; see details in the Supporting Information) in order to control polymer growth and molecular weight (MW), while minimizing reaction times, and were

Scheme 2. Synthesis of the PBDT(T)TPD(CO)(R_1/R_2) Derivatives with Branched 2-Ethylhexyl (2EH) Side Chains on the BDT(T) Motifs and Linear Alkyl Side Chains of Varying Length (C1, C3, C7, C11, C13) on TPD(CO)

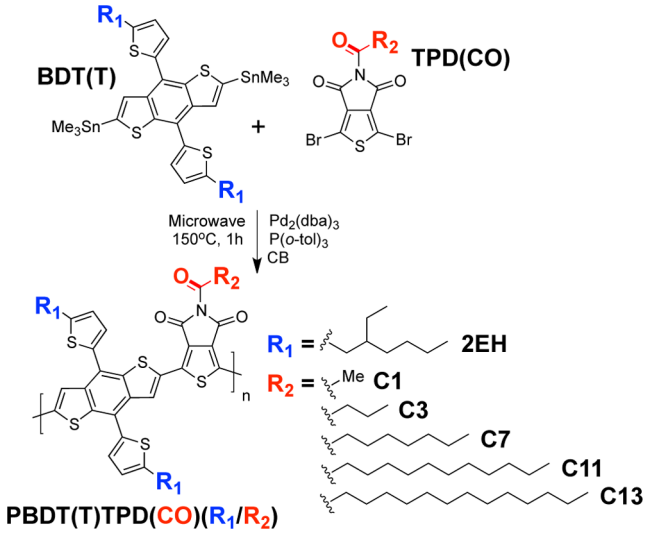

dx.doi.org/10.1021/cm5002303 | *Chem. Mater.* 2014, 26, 2829−2835

purified using established methods.[2,4] A batch of PBDT(T)-TPD(2EH/C8) was also polymerized to serve as a model polymer in this study (see details in the Supporting Information). The size exclusion chromatography (SEC)-estimated polymers' molecular weights and the thermogravimetric analyses (TGA) of the polymers are provided in the Supporting Information (Table S1, and Figure S3).

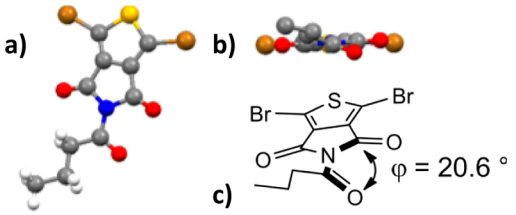

Figure 1. (a) Molecular conformation of TPD(CO)(C3) resolved by single-crystal X-ray; and (b) in-plane conformation. (c) Schematic illustrating the torsion angle of 20.6° between the *N*-alkyloyl substituent and the plane of the imide.

Optical Absorption and Ionization Energies. The optical absorption spectra of the *N*-alkyloyl-substituted PBDT-(T)TPD(CO)(2EH/C7) analogue and that of its counterpart PBDT(T)TPD(2EH/C8) are shown in Figure 2a, and Figure 2b provides the ionization potentials (IP) of the polymers measured by photoelectron spectroscopy in air (PESA). Comparing the spectral absorption of the two polymers, the absorption onsets and maxima in both solutions and thin films of PBDT(T)TPD(CO) reflect net bathochromic shifts (ca. 60 nm). With optical gaps (E_{opt}) estimated from the onsets of the thin-film absorptions, PBDT(T)TPD(CO)(2EH/C7) is found to be a lower-optical-gap material: 1.79 vs 1.88 eV for the model polymer PBDT(T)TPD(2EH/C8). In parallel, from Figure 2b, it should be noted that the IP of PBDT(T)TPD-(CO)(2EH/C7), 5.41 eV, is slightly larger than that of its PBDT(T)TPD(2EH/C8) counterpart, 5.29 eV—a result that, at a first level of approximation, can account for a lower-lying HOMO. In turn, it can be inferred that the *N*-alkyloyl substitution promotes a lower-lying LUMO in PBDT(T)TPD-(CO)(2EH/C7), which would be the main contributor to a reduced HOMO−LUMO gap.

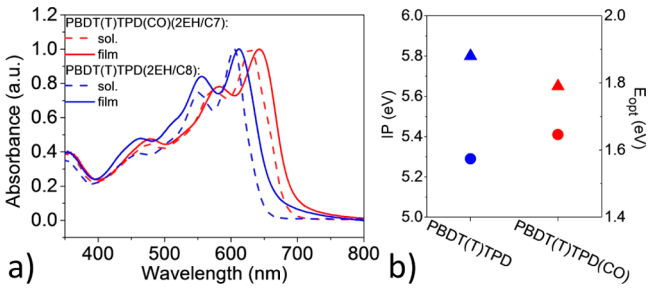

Figure 2. (a) Superimposed UV−vis optical absorption spectra (solution and film) of PBDT(T)TPD(CO)(2EH/C7) and its counterpart PBDT(T)TPD(2EH/C8). (b) PESA-estimated ionization potentials (IP, circles) and optical band gap (E_{opt}, triangles) estimated from the onset of the UV−vis absorption spectra (films) for the two polymer analogues.

Device Testing and Characterization. Thin-film BHJ solar cells with the standard configuration ITO/PEDOT:PSS/PBDT(T)TPD(CO):$PC_{71}BM$/Ca/Al were fabricated and tested under AM1.5G solar illumination (100 mW/cm^2). The cells with optimized PBDT(T)TPD(CO):$PC_{71}BM$ blend ratios (1:1, wt/wt) were cast from chloroform (CF); similar device fabrication and optimization procedures were used for all of the PBDT(T)TPD(CO) derivatives (see the Supporting Information).

As shown in Table 1, "*as-cast*" BHJ solar cells made from blends of the PBDT(T)TPD(CO) analogues and $PC_{71}BM$ achieved moderate to low PCEs, ranging from 3.9% (max. 4.1%) for the (2EH/C1) derivative, down to only 1.5% (max. 1.7%) for the (2EH/C13) analogue. Interestingly, as illustrated in Figure 3b, the solar cell PCE decreases almost linearly with increasing side-chain length on the TPD(CO) motifs, mainly due to a drastic drop in device short-circuit current (J_{SC}) across the device set (see Table 1, 8.7 → 4.3 mA/cm^2). These devices show modest fill factors (FF) within the range of 37−45%, but high V_{OC} values > 1 V, in agreement with the large PESA-estimated IP of the PBDT(T)TPD(CO) polymer analogues (Figure 2b). Thus, the V_{OC} values achieved with PBDT(T)-TPD(CO)-based devices are found to be greater than that obtained with their PBDT(T)TPD counterparts (V_{OC} ~ 1 V) by at least 0.04 eV, and by up to 0.09 eV. The current density−

Table 1. PV Performance of the PBDT(T)TPD(CO) Derivatives in Standard BHJ Devices with $PC_{71}BM$[a,d]

polymer analogues	CN, DIO	J_{SC} [mA/cm^2]	V_{OC} [V]	FF	avg. PCE [%]	max. PCE [%]
TPD(CO); (2EH/C1)		8.7	1.04	0.45	3.9	4.1
	3%[b]	10.3	1.05	0.57	5.9	6.1
TPD(CO); (2EH/C3)		7.8	1.09	0.45	3.6	3.8
	3%[b]	10.7	1.08	0.57	6.3	6.5
TPD(CO); (2EH/C7)		6.6	1.05	0.39	2.6	2.7
	3%[b]	10.6	1.05	0.60	6.5	6.7
TPD(CO); (2EH/C11)		4.6	1.04	0.40	1.8	2.0
	3%[b]	7.7	1.06	0.57	4.4	4.6
TPD(CO); (2EH/C13)		4.3	1.06	0.37	1.5	1.7
	3%[b]	7.0	1.05	0.56	3.8	4.1
TPD; (2EH/C8)		3.5	1.00	0.44	1.4	1.5
	3%[c]	11.1	1.00	0.58	6.1	6.5

[a]Optimized devices with a polymer:$PC_{71}BM$ ratio of 1:1 (w/w). All devices were solution-cast from chloroform (CF). [b]Devices prepared from blends containing 3% (v/v) of the processing additive 1-chloronaphthalene (CN). [c]Devices prepared from blends containing 3% (v/v) of the processing additive 1,8-diiodooctane (DIO). [d]Additional device statistics, including variances, are provided in the Supporting Information (Figure S5).

dx.doi.org/10.1021/cm5002303 | *Chem. Mater.* 2014, 26, 2829−2835

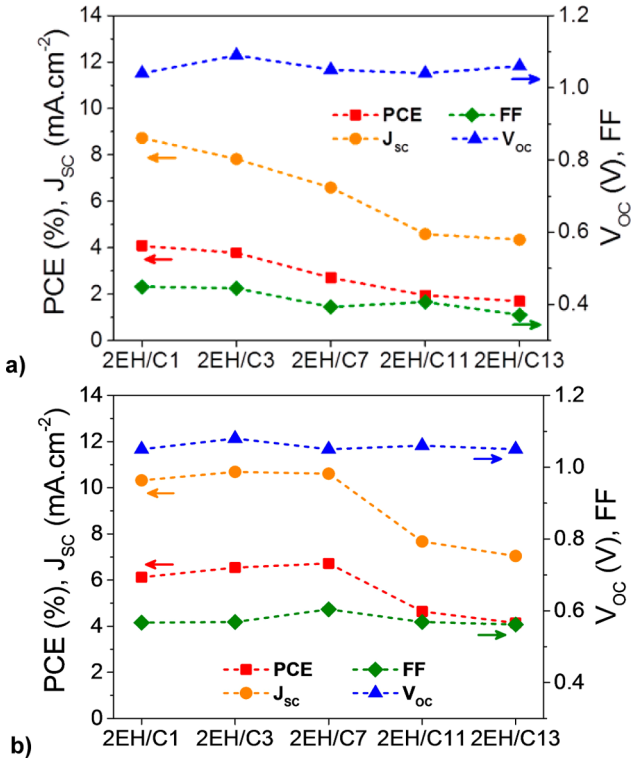

Figure 3. Evolution of the figures of merit (J_{SC}, V_{OC}, FF, PCE) for optimized BHJ solar cells fabricated from the PBD(T)TPD(CO) derivatives—(2EH/C1), (2EH/C3), (2EH/C7), (2EH/C11), and (2EH/C13)—under AM1.5G: (a) Devices cast from CF, no CN additive; (b) with 3% CN additive (v/v). Additional device statistics, including variances, are provided in the Supporting Information (Figure S5).

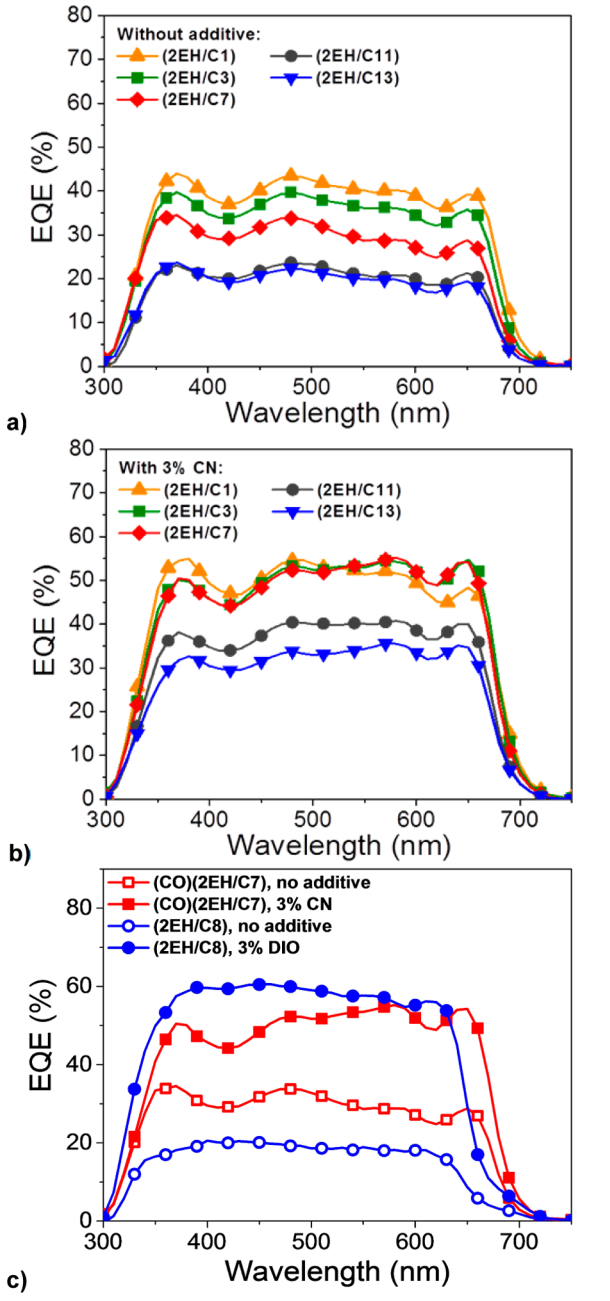

Figure 4. Superimposed EQE spectra of optimized BHJ devices fabricated from the PBDT(T)TPD(CO) derivatives: (a) no CN additive; (b) with 3% CN (v/v). (c) Superimposed EQE spectra of optimized BHJ devices of PBDT(T)TPD(CO) and its counterpart PBDT(T)TPD (model polymer); no CN/DIO additive (empty symbols), and with 3% CN/DIO (v/v) (full symbols).

voltage (J–V) curves of the optimized PBDT(T)TPD(CO)-based devices and the external quantum efficiency (EQE) spectra of optimized devices of the five polymer analogues are shown in Figure S4a (Supporting Information) and Figure 4a. While comparably broad in the range of 350–680 nm, the EQE response of the (2EH/C1)-based device is shown to be greater than that of the device cast with (2EH/C3) by ca. 4%, and greater than that of the (2EH/C7)-based device by ca. 10% within this range. In parallel, the EQE response of the (2EH/C1)-based device averaged over the range of 350–680 nm is approximately 2 times greater than that of the devices made with (2EH/C11) and (2EH/C13), suggesting that "*as-cast*" BHJs of (2EH/C11) and (2EH/C13) may be hindered by morphological effects (vide infra) and inefficient charge separation/extraction. Overall, the EQEs of the (2EH/C11)- and (2EH/C13)-based solar cells remain under 25% across the visible spectrum, in agreement with the comparably low device J_{SC} values obtained with these polymer analogues (<5 mA/cm^2). As illustrated in Figure 4c, it is worth noting that the EQE response of PBDT(T)TPD(CO) extends beyond that of its PBDT(T)TPD counterpart by ca. 50 nm—an observation that is consistent with the distinct onsets of absorption of the polymers (Figure 2a). Estimated from the space charge limited current (SCLC) model, the hole mobilities of PBDT(T)TPD-(CO)(2EH/C7), 2.0×10^{-4} cm^2 V^{-1} s^{-1} (see the Supporting Information, Figure S6), are on the same order of magnitude as those measured in previous work for its PBDT(T)TPD(2EH/C8) counterpart, 4.7×10^{-4} cm^2 V^{-1} s^{-1}.[13] Thus, other parameters must come into play to explain the relatively low J_{SC} and FF values in "*as-cast*" BHJ solar cells with PBDT(T)TPD-(CO) polymers.

The BHJ morphologies of optimized devices of PBDT(T)-TPD(CO)(2EH/C1), PBDT(T)TPD(CO)(2EH/C7), and PBDT(T)TPD(CO)(2EH/C13) were examined by bright-field transmission electron microscopy (TEM) (see details in the Supporting Information); analyses are shown in Figure 5a–c. While the BHJ thin film cast with the (2EH/C1) derivative shows a relatively well-mixed BHJ morphology (Figure 5a), the two other BHJ thin films show a net degree of phase separation between polymer and fullerene, yet on different length scales: ~50 nm (avg.) in PBDT(T)TPD(CO)(2EH/C7):$PC_{71}BM$,

dx.doi.org/10.1021/cm5002303 | *Chem. Mater.* 2014, 26, 2829–2835

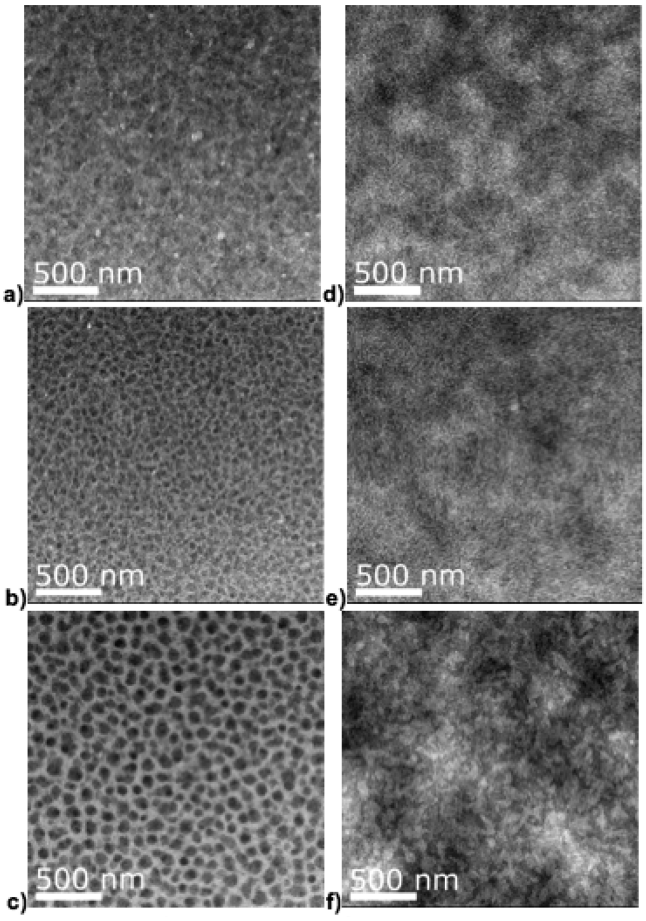

Figure 5. Bright-field TEM images of the thin-film morphologies in optimized BHJs of (a) PBDT(T)TPD(CO)(2EH/C1), no CN additive; (b) the (2EH/C7) analogue, no CN; (c) the (2EH/C13) analogue; no CN; (d) PBDT(T)TPD(CO)(2EH/C1), 3% CN (v/v); (e) the (2EH/C7) analogue, 3% CN (v/v); and (f) the (2EH/C13) analogue; 3% CN (v/v). Dark areas: PCBM-rich domains; clear areas: polymer-rich domains.

and within range of 100−150 nm in PBDT(T)TPD(CO)-(2EH/C13):$PC_{71}BM$ blend films. In bright-field TEM, darker areas can be attributed to the PCBM-rich regions, here interconnected via a network of polymer-rich boundaries. It is worth noting that (i) none of these thin-film morphologies compare to the type of fibrillar networks achieved in efficient BHJ devices cast from PBDTTPD(2EH/C8),[32] and (ii) the coarsely phase-separated morphology in PBDT(T)TPD(CO)-(2EH/C13):$PC_{71}BM$ blend films (see higher-magnification TEM images in the Supporting Information, Figure S7) is likely to limit the efficiency of exciton diffusion to the donor−acceptor domain boundaries, in turn, yielding low device photocurrents and poor BHJ solar cell efficiencies. These observations are consistent with the respectable PCE of PBDT(T)TPD(CO)(2EH/C1)-based devices (avg. 3.9%; max. 4.1%), and with the notably lower PCE of the BHJ solar cells made with the (2EH/C13) derivative (avg. 1.5%; max. 1.7%).

Small-molecule additives mixed in the polymer:PCBM blend solution, such as 1-chloronaphthalene (CN) and 1,8-diiodooctane (DIO), have previously been shown to help mitigate the thin-film morphology in BHJ solar cells.[33−36] The optimized BHJ morphologies can result in remarkable photocurrent increases, leading to net improvements in solar cell efficiency.[33−36] In light of the relatively coarse phase-separated patterns discussed above for "*as-cast*" devices, solar cells were also fabricated from blend solutions containing optimum concentrations of CN additive (3%, v/v); the results are summarized in Table 1. As illustrated in Figure 3b, all the BHJ thin films cast from blends containing CN achieved higher J_{SC} and greater FFs, yielding significant improvements in device PCE. While "*as-cast*" solar cells made with the PBDT(T)TPD-(CO) derivatives showed only modest FFs in the range of 37−45% (Figure 3a), the devices cast from CN-containing solutions reach higher FFs of 56−60% (i.e., +12−21%), while maintaining their high V_{OC} > 1 V. In particular, J_{SC} values > 10 mA/cm^2 can be measured for the shorter-chain polymers: 10.3, 10.7, and 10.6 mA/cm^2 with the (2EH/C1), (2EH/C3), and (2EH/C7) analogues, respectively. Combined with FFs of ca. 60%, optimized BHJ devices cast with PBDT(T)TPD-(CO)(2EH/C7) reach 6.7% PCE (avg. 6.5%), which represents a ca. 2.5-fold increase in PCE relative to "*as-cast*" BHJ devices. The current density−voltage (J−V) curves of the optimized PBDT(T)TPD(CO) devices cast from CN-containing blends and the external quantum efficiency (EQE) spectra of optimized devices of the five polymer analogues are shown in Figure S4b (Supporting Information) and Figure 4b. The EQE responses of the (2EH/C1)-, (2EH/C3)-, and (2EH/C7)-based devices are comparable in the range of 350−680 nm, averaging ca. 50% across this range. In contrast, the EQEs of the (2EH/C11)- and (2EH/C13)-based solar cells remain within the range of 30−40% across the visible spectrum, correlating with lower device J_{SC} values (<8 mA/cm^2). As shown in Figure 5d−f, in examining the thin-film morphologies of the solar cells cast from the (2EH/C1), (2EH/C7), and (2EH/C13) analogues in blends with $PC_{71}BM$ and CN (3%), it should be noted that the relatively coarse network of polymer- and PCBM-rich domains visible earlier in the (2EH/C1)- and (2EH/C7)-based BHJ thin films is no longer apparent. The much finer patterns observed for these two derivatives point to a more intimately mixed polymer:$PC_{71}BM$ blend morphology. In parallel, optimized BHJ solar cells of the (2EH/C1) and (2EH/C7) analogues with CN tend to yield higher J_{SC} values (see Table 1, 8.7 → 10.3 mA/cm^2 and 6.6 → 10.6 mA/cm^2, respectively). Meanwhile, Figure 5f shows that BHJ thin films of the (2EH/C13) derivative retain a certain degree of apparent phase separation, which may be at the origin of the lower photocurrents and EQE of the solar cells.

Overall, BHJ solar cells fabricated from PBDT(T)TPD-(CO)(2EH/C7) achieved figures of merit comparable to those of the model polymer PBDT(T)TPD(2EH/C8) (Table 1), yet it is worth noting from Figure 4c that the EQE of the PBDT(T)TPD(CO)(2EH/C7)-based device does not match that of its PBDT(T)TPD(2EH/C8) counterpart in the short-wavelength region (350−550 nm). Excitons recombining on the fullerene could explain the lower EQE of the device in this range dominated by PCBM absorption.[3] Comparing the texture of PBDT(T)TPD(CO)(2EH/C7) and PBDT(T)TPD(2EH/C8) by grazing incidence X-ray scattering (GIXS) (see the Supporting Information, Figure S8a: neat polymer films), the two analogues show comparable scattering patterns, with a partial arc at $q \approx 1.72$ Å^{-1} along the out-of-plane direction ($q_{xy} \approx 0$), indicating the presence of "face-on"-oriented π-aggregates (stacking "out-of-plane", π−π spacing: ca. 3.65 and 3.68 Å, in PBDT(T)TPD(CO)(2EH/C7) and PBDT(T)TPD(2EH/C8), respectively). While "face-on" polymer orientations have

been suggested to promote BHJ solar cell efficiency,[4,37−41] the scattering intensity at $q \approx 1.72$ Å^{-1} in the optimized BHJ thin films of the PBDT(T)TPD(CO) derivatives and PCBM (see the Supporting Information, Figure S8b: BHJ thin films) is not as pronounced as in the neat films, suggesting that the presence of oriented π-aggregates is not a determining factor in PBDT(T)TPD(CO)-based BHJ device performance.

■ CONCLUSIONS

In summary, we have shown that electron-deficient *N*-alkyloyl-substituted TPD motifs (TPD(CO)) can lower both the LUMO and the HOMO levels of the polymer donor PBDT(T)TPD, yielding device V_{OC} > 1 V (up to ca. 1.1 V) in standard BHJ solar cells with $PC_{71}BM$. Despite the high V_{OC} achieved (i.e., low polymer HOMO), BHJ solar cells cast with PBDT(T)TPD(CO) polymers in blend solutions containing the small-molecule additive CN (3%) can reach J_{SC} values > 10 mA/cm^2, FFs on the order of 60%, and PCEs of up to 6.7%. The significant improvements in J_{SC}, FFs (up to +21%), and overall PCE obtained with optimized devices cast from CN-containing blends appear to result from finer BHJ morphologies compared to that of "as-cast" solar cells. With their relatively wide optical band gaps ($E_{opt} \sim 1.8$ eV), PBDT(T)-TPD(CO) analogues are promising systems for use in the high-band-gap cell of tandem solar cells.

■ ASSOCIATED CONTENT

Ⓢ Supporting Information

Synthetic details, monomer and polymer characterizations, device fabrication protocols and statistics, SCLC mobility plots, higher-magnification TEM images, and GIXS patterns. This material is available free of charge via the Internet at http://pubs.acs.org.

■ AUTHOR INFORMATION

Corresponding Author

*E-mail: pierre.beaujuge@kaust.edu.sa.

Notes

The authors declare no competing financial interests.

■ ACKNOWLEDGMENTS

The authors acknowledge financial support under Baseline Research Funding from King Abdullah University of Science and Technology (KAUST). The authors thank KAUST Analytical Core Laboratories for mass spectrometry, SEC measurements, and elemental analyses, and Sandra Seywald (MPIP − Mainz, Germany) for additional SEC measurements. The authors thank the Advanced Imaging and Characterization Laboratories at KAUST for technical support. Portions of this research were carried out at the Stanford Synchrotron Radiation Lightsource user facility, operated by Stanford University on behalf of the U.S. Department of Energy, Office of Basic Energy Sciences.

■ REFERENCES

(1) Beaujuge, P. M.; Frechet, J. M. J. *J. Am. Chem. Soc.* **2011**, *133*, 20009−20029.
(2) Cabanetos, C.; El Labban, A.; Bartelt, J. A.; Douglas, J. D.; Mateker, W. R.; Frechet, J. M. J.; McGehee, M. D.; Beaujuge, P. M. *J. Am. Chem. Soc.* **2013**, *135*, 4656−4659.
(3) Hoke, E. T.; Vandewal, K.; Bartelt, J. A.; Mateker, W. R.; Douglas, J. D.; Noriega, R.; Graham, K. R.; Fréchet, J. M. J.; Salleo, A.; McGehee, M. D. *Adv. Energy Mater.* **2013**, *3*, 220−230.
(4) Piliego, C.; Holcombe, T. W.; Douglas, J. D.; Woo, C. H.; Beaujuge, P. M.; Fréchet, J. M. J. *J. Am. Chem. Soc.* **2010**, *132*, 7595−7597.
(5) Zhou, H.; Yang, L.; You, W. *Macromolecules* **2012**, *45*, 607−632.
(6) Mei, J.; Bao, Z. *Chem. Mater.* **2014**, *26*, 604−615.
(7) Lei, T.; Wang, J.-Y.; Pei, J. *Chem. Mater.* **2014**, *26*, 594−603.
(8) Bronstein, H.; Leem, D. S.; Hamilton, R.; Woebkenberg, P.; King, S.; Zhang, W. M.; Ashraf, R. S.; Heeney, M.; Anthopoulos, T. D.; de Mello, J.; McCulloch, I. *Macromolecules* **2011**, *44*, 6649−6652.
(9) Huo, L.; Zhang, S.; Guo, X.; Xu, F.; Li, Y.; Hou, J. *Angew. Chem., Int. Ed.* **2011**, *50*, 9697−9702.
(10) Dou, L.; Gao, J.; Richard, E.; You, J.; Chen, C.-C.; Cha, K. C.; He, Y.; Li, G.; Yang, Y. *J. Am. Chem. Soc.* **2012**, *134*, 10071−10079.
(11) Zhang, Y.; Gao, L.; He, C.; Sun, Q.; Li, Y. *Polym. Chem.* **2013**, *4*, 1474−1481.
(12) Dong, Y.; Hu, X.; Duan, C.; Liu, P.; Liu, S.; Lan, L.; Chen, D.; Ying, L.; Su, S.; Gong, X.; Huang, F.; Cao, Y. *Adv. Mater.* **2013**, *25*, 3683−3688.
(13) Warnan, J.; Labban, A. E.; Cabanetos, C.; Hoke, E.; Shukla, P. K.; Risko, C.; Brédas, J.-L.; McGehee, M. D.; Beaujuge, P. M. *Chem. Mater.* **2014**, *26*, 2299−2306.
(14) Huo, L.; Ye, L.; Wu, Y.; Li, Z.; Guo, X.; Zhang, M.; Zhang, S.; Hou, J. *Macromolecules* **2012**, *45*, 6923−6929.
(15) Wang, Y.; Yang, F.; Liu, Y.; Peng, R.; Chen, S.; Ge, Z. *Macromolecules* **2013**, *46*, 1368−1375.
(16) Zhang, M.; Gu, Y.; Guo, X.; Liu, F.; Zhang, S.; Huo, L.; Russell, T. P.; Hou, J. *Adv. Mater.* **2013**, *25*, 4944−4949.
(17) Yuan, J.; Zhai, Z.; Dong, H.; Li, J.; Jiang, Z.; Li, Y.; Ma, W. *Adv. Funct. Mater.* **2013**, *23*, 885−892.
(18) Bijleveld, J. C.; Verstrijden, R. A. M.; Wienk, M. M.; Janssen, R. A. J. *Appl. Phys. Lett.* **2010**, *97*, 073304−073303.
(19) Najari, A.; Berrouard, P.; Ottone, C.; Boivin, M.; Zou, Y.; Gendron, D.; Caron, W.-O.; Legros, P.; Allen, C. N.; Sadki, S.; Leclerc, M. *Macromolecules* **2012**, *45*, 1833−1838.
(20) Chen, H.-Y.; Hou, J.; Zhang, S.; Liang, Y.; Yang, G.; Yang, Y.; Yu, L.; Wu, Y.; Li, G. *Nat. Photonics* **2009**, *3*, 649−653.
(21) Liang, Y.; Feng, D.; Wu, Y.; Tsai, S.-T.; Li, G.; Ray, C.; Yu, L. *J. Am. Chem. Soc.* **2009**, *131*, 7792−7799.
(22) Hou, J.; Chen, H.-Y.; Zhang, S.; Chen, R. I.; Yang, Y.; Wu, Y.; Li, G. *J. Am. Chem. Soc.* **2009**, *131*, 15586−15587.
(23) Liang, Y.; Yu, L. *Acc. Chem. Res.* **2010**, *43*, 1227−1236.
(24) Zou, Y.; Najari, A.; Berrouard, P.; Beaupré, S.; Réda Aich, B.; Tao, Y.; Leclerc, M. *J. Am. Chem. Soc.* **2010**, *132*, 5330−5331.
(25) Guo, X.; Ortiz, R. P.; Zheng, Y.; Kim, M.-G.; Zhang, S.; Hu, Y.; Lu, G.; Facchetti, A.; Marks, T. J. *J. Am. Chem. Soc.* **2011**, *133*, 13685−13697.
(26) Beaupré, S.; Najari, A.; Leclerc, M. *Synth. Met.* **2013**, *182*, 9−12.
(27) Wang, M.; Hu, X.; Liu, P.; Li, W.; Gong, X.; Huang, F.; Cao, Y. *J. Am. Chem. Soc.* **2011**, *133*, 9638−9641.
(28) Wang, Y.; Yang, F.; Liu, Y.; Peng, R. X.; Chen, S. J.; Ge, Z. Y. *Macromolecules* **2013**, *46*, 1368−1375.
(29) Wu, Y.; Li, Z.; Ma, W.; Huang, Y.; Huo, L.; Guo, X.; Zhang, M.; Ade, H.; Hou, J. *Adv. Mater.* **2013**, *25*, 3449−3455.
(30) Dou, L.; Chang, W.-H.; Gao, J.; Chen, C.-C.; You, J.; Yang, Y. *Adv. Mater.* **2013**, *25*, 825−831.
(31) Yuan, J.; Zhai, Z.; Li, J.; Lu, J.; Huang, X.; Xu, Z.; Ma, W. *J. Mater. Chem. A* **2013**, *1*, 12128−12136.
(32) Bartelt, J. A.; Beiley, Z. M.; Hoke, E. T.; Mateker, W. R.; Douglas, J. D.; Collins, B. A.; Tumbleston, J. R.; Graham, K. R.; Amassian, A.; Ade, H.; Fréchet, J. M. J.; Toney, M. F.; McGehee, M. D. *Adv. Energy Mater.* **2013**, *3*, 364−374.
(33) Peet, J.; Kim, J. Y.; Coates, N. E.; Ma, W. L.; Moses, D.; Heeger, A. J.; Bazan, G. C. *Nat. Mater.* **2007**, *6*, 497−500.
(34) Lee, J. K.; Ma, W. L.; Brabec, C. J.; Yuen, J.; Moon, J. S.; Kim, J. Y.; Lee, K.; Bazan, G. C.; Heeger, A. J. *J. Am. Chem. Soc.* **2008**, *130*, 3619−3623.
(35) Hoven, C. V.; Dang, X.-D.; Coffin, R. C.; Peet, J.; Nguyen, T.-Q.; Bazan, G. C. *Adv. Mater.* **2010**, *22*, E63−E66.

(36) Woo, C. H.; Beaujuge, P. M.; Holcombe, T. W.; Lee, O. P.; Fréchet, J. M. J. *J. Am. Chem. Soc.* **2010**, *132*, 15547−15549.
(37) Guo, J.; Liang, Y.; Szarko, J.; Lee, B.; Son, H. J.; Rolczynski, B. S.; Yu, L.; Chen, L. X. *J. Phys. Chem. B* **2010**, *114*, 742−748.
(38) Yiu, A. T.; Beaujuge, P. M.; Lee, O. P.; Woo, C. H.; Toney, M. F.; Fréchet, J. M. J. *J. Am. Chem. Soc.* **2011**, *134*, 2180−2185.
(39) Kim, D. H.; Ayzner, A. L.; Appleton, A. L.; Schmidt, K.; Mei, J.; Toney, M. F.; Bao, Z. *Chem. Mater.* **2012**, *25*, 431−440.
(40) Osaka, I.; Kakara, T.; Takemura, N.; Koganezawa, T.; Takimiya, K. *J. Am. Chem. Soc.* **2013**, *135*, 8834−8837.
(41) Guo, X.; Zhou, N.; Lou, S. J.; Smith, J.; Tice, D. B.; Hennek, J. W.; Ortiz, R. P.; Navarrete, J. T. L.; Li, S.; Strzalka, J.; Chen, L. X.; Chang, R. P. H.; Facchetti, A.; Marks, T. J. *Nat. Photonics* **2013**, *7*, 825−833.